# Motional Finite Element Simulation of Magnetic Brakes and Solid Rotor Induction Machines

Herbert De Gersem,[*] Kay Hameyer[†]

April 25, 2002

### Abstract

The torques of a magnetic brake and a solid rotor induction machine, fed by sinusoidal voltage sources, are simulated by a motional finite element method. Oscillatory solutions occurring for motional models with elevated velocities, are prevented by adaptive mesh refinement relying upon intermediate solutions stabilised by upwinded finite element test functions. A relaxed successive approximation deals with the non-linear material properties. The connections of the conductors and windings within the finite element model to external loads, impedances and supplies are represented by an electric circuit and added to the system of equations. The technical examples indicate the advantages of the motional formulation.

## 1 Introduction

A conductive material moving in a magnetic field experiences eddy currents [1]. For increasing speeds, the eddy currents are pushed towards the surface of the conductive material in the downwind direction, i.e. the direction of the velocity. The reverse direction is called the upwind direction. The currents generate forces and Joule losses. There are numerous applications of motional eddy currents, e.g. induction machines, magnetic brakes [2], magnetic levitation or suspension devices and non-destructive testing tools [3]. The accurate simulation of motional effects, however, is still challenging. Transient finite element simulation is a common practice, but suffers from excessive computation times, especially for models with complicated geometries and models experiencing small skin depths, which both require fine meshes. Two alternatives are possible but are based on specific assumptions. If the magnetic field at the interface between the moving bodies features a particular regularity, the motional effects can be simulated by a non-motional formulation relying upon the slip transformation technique [4]. This approach is applicable to three-phase induction machines. For models with uniformly moving parts, such as solid rotor induction machines and

[*]H. De Gersem is with the Technische Universität Darmstadt, Computational Electromagnetics Laboratory, Schloßgartenstraße 8, D-64289 Darmstadt, Germany (e-mail: degersem@temf.tu-darmstadt.de).

[†]K. Hameyer is with the Katholieke Universiteit Leuven, Dep. ESAT, Div. ELECTA, Kasteelpark Arenberg 10, B-3001 Leuven-Heverlee, Belgium (e-mail: kay.hameyer@esat.kuleuven.ac.be).

electromagnetic rail braking systems, the motional eddy currents can be accounted for by an additional, motional term in the partial differential equation [5]. For the steady-state simulation of these devices, a motional formulation is preferred over a transient one because time stepping, which is expensive for large models, is avoided. In this paper, the motional formulation is equipped with an adaptive mesh refinement strategy, an upwinding technique, a relaxed non-linear loop and an external circuit coupling mechanism, which are required to apply the formulation to technical models.

## 2  Motional finite element formulation

A rigid body is said to be uniform with respect to its movement if the movement does not change the configuration of the model. This requires the moving bodies to be infinitely long in the direction of the motion and to have a constant cross-section perpendicular to the velocity vector. In the case of translation, the moving body corresponds to an arbitrary cross-section extruded along the direction of the motion. Examples are rail braking systems for high speed trains [5] and linear induction motors with a solid translators [6]. In the case of rotational movement, the moving body consists of concentric tubes. This is true for the rotational magnetic brake and the solid rotor induction machine considered as examples here.

The formulation for the steady-state simulation of motional eddy currents in uniformly moving bodies, is derived by introducing the magnetic vector potential $\mathbf{A}$ and the electric voltage $V$ into the Maxwell equations. Because the excitations are sinusoidal in time, it is convenient to represent all field quantities by the phasors $\underline{\mathbf{A}}$ and $\underline{V}$:

$$\mathbf{A} = \mathrm{Re}\left\{\underline{\mathbf{A}}e^{\mathrm{j}\omega t}\right\} ; \tag{1}$$

$$V = \mathrm{Re}\left\{\underline{V}e^{\mathrm{j}\omega t}\right\} \tag{2}$$

with $\omega$ the electric pulsation. The laws of Ampère and Faraday-Lenz are combined yielding one single partial differential equation

$$\nabla \times (\nu\nabla \times \underline{\mathbf{A}}) + \sigma\mathbf{u} \times \nabla \times \underline{\mathbf{A}} + \mathrm{j}\omega\sigma\underline{\mathbf{A}} = -\sigma\nabla\underline{V} \tag{3}$$

with $\mathbf{u}$ the velocity, $\nu$ the reluctivity and $\sigma$ the conductivity. The devices considered here, are simulated by 2D, cartesian models. The cross-section of a device by the $(x, y)$-plane is denoted by $\Omega$. The electric excitation is perpendicular to $\Omega$. Therefore, the magnetic vector potential has only a $z$-component, i.e. $\underline{\mathbf{A}} = (0, 0, \underline{A}_z)$. The cross-sections of the devices are triangulated. Linear finite elements $N_j(x, y)$ are associated with the vertices $j = 1, \ldots, n$ of the finite element mesh. The finite element solution for $\underline{A}_z$ is a linear combination of $N_j(x, y)$ with the corresponding coefficients $\underline{A}_{z,j}$ solved from

$$[k_{ij} + m_{ij} + l_{ij}]\left[\underline{A}_{z,j}\right] = \left[\underline{f}_i\right] \tag{4}$$

where

$$k_{ij} = \int_\Omega \nu \left(\frac{\partial N_i}{\partial x}\frac{\partial N_j}{\partial x} + \frac{\partial N_i}{\partial y}\frac{\partial N_j}{\partial y}\right) \mathrm{d}\Omega ; \tag{5}$$
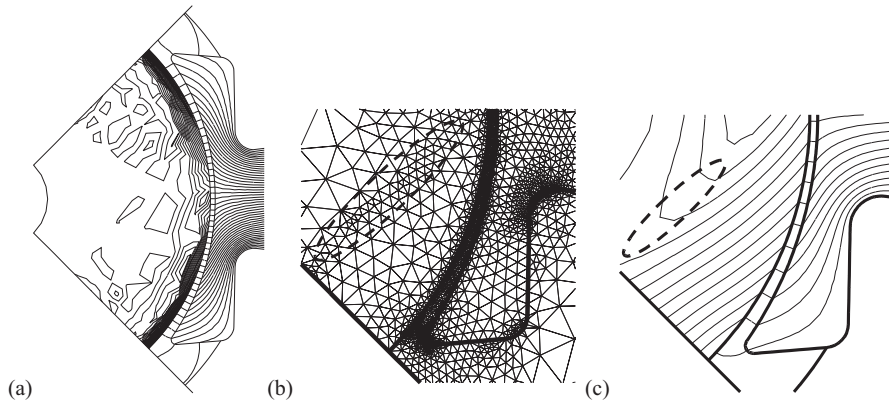
Figure 1: (a) Finite element solution of a convection dominated problem; (b) non-uniformly refined mesh achieved by the combined upwinding, adaptive mesh refinement approach and (c) detail of a magnetic flux lines on the refined mesh (the ellips indicates a transition layer of the magnetic field).

$$m_{ij} \quad = \quad \int_\Omega \sigma \left( v_x \frac{\partial N_j}{\partial x} + v_y \frac{\partial N_j}{\partial y} \right) N_i \, \mathrm{d}\Omega \; ; \tag{6}$$

$$l_{ij} \quad = \quad \int_\Omega \mathrm{j}\omega\sigma N_i N_j \, \mathrm{d}\Omega \; ; \tag{7}$$

$$\underline{f}_i \quad = \quad - \int_\Omega \sigma \nabla \underline{V} N_i \, \mathrm{d}\Omega \; . \tag{8}$$

The system matrix is sparse, but because of the presence of $m_{ij}$, not symmetric. The system is solved by preconditioned Krylov subspace solvers such as e.g. Bi-Conjugate Gradients Stabilised and Generalised Minimal Residual with a Successive Over-Relaxation preconditioner [7].

## 3  Upwinding combined with adaptive mesh refinement

The governing partial differential equation (3) is a convection-diffusion equation. For this type of equations, it is known that the finite element solution is numerically unstable, i.e. may contain spurious oscillations, if the convection is dominant over the diffusion [8] (Fig. 1a). A sufficient but not strictly necessary condition for numerical stability is

$$\mathrm{Pe} = \frac{\sigma \, |\mathbf{u}| \, h}{2\nu} < 1 \tag{9}$$

where Pe is called the *Péclet number* according to the characteristic mesh size $h$ of the finite element discretisation.

Equation (9) already indicates two possible techniques to cure the numerical problem: decreasing the mesh size and/or decreasing the ratio $\sigma|\mathbf{u}|/\nu$. The first approach may lead to unacceptably large models. The second approach changes the original

differential problem. Here, a combination of both techniques is proposed [9]. The reluctivity is artificially augmented by the *additional* reluctivity $\nu_{\mathrm{add}}$, yielding the *artificial* diffusion coefficient $\nu_{\mathrm{art}} = \nu + \nu_{\mathrm{add}}$. $\nu_{\mathrm{add}}$ is chosen such that $\sigma|\mathbf{u}|h/2\nu_{\mathrm{art}} < 1$, which ensures a non-oscillatory solution even on a coarse mesh. The artificial diffusion approach is equivalent to a particular way of stabilising the finite element method by applying *upwinded* test functions, i.e. test functions getting more weight in the upwind direction [8]. Although the finite element solution obtained by upwinding is too diffusive, it indicates the places where large eddy currents, and hence, steep transitions of the magnetic vector potential, occur. This enables an error estimator to mark the corresponding elements for refinement. An error estimator applied to the oscillating solution of Fig. 1a would pass a non-reliable advise to the refinement algorithm. At the transition layers the mesh size decreases and as a consequence, the need for upwinding vanishes. The parts of the moving conductors far away from the downwind boundary feature an almost constant magnetic vector potential and are not refined by the algorithm. They are excluded for upwinding when the transition layers at the downwind boundaries are sufficiently localised. This particular combination of adaptive mesh refinement and upwinding yields accurate solutions on relatively small finite element meshes. The strategy results in non-uniform mesh refinement, which is advantageous for technical models commonly featuring complicated geometries and local motional eddy current effects (Fig. 1b and Fig. 1c).

## 4    Field-circuit coupling

The stator coils are connected to a voltage supply and to lumped parameters that model the resistances and inductances of the end windings. The currents through the rotor parts are forced to zero. The additional equations modelling these external circuit couplings, are added to the finite element system:

$$
\begin{bmatrix}
k_{ij} + m_{ij} + l_{ij} & \hat{f}_{iq} & \tilde{f}_{ib} \\
\hat{m}_{pj} + \hat{l}_{pj} & r_{pq} & 0 \\
\tilde{m}_{aj} + \tilde{l}_{aj} & 0 & g_{ab}
\end{bmatrix}
\begin{bmatrix}
\underline{A}_{z,j} \\
\underline{i}_q \\
\underline{v}_b
\end{bmatrix}
=
\begin{bmatrix}
0 \\
\underline{v}_p \\
0
\end{bmatrix}
\tag{10}
$$

where

$$
\hat{f}_{iq} = -\int_{\Omega_q} \frac{N_q}{S_q} N_i \, \mathrm{d}\Omega \; ;
\tag{11}
$$

$$
\tilde{f}_{ib} = -\int_{\Omega_b} \frac{\sigma}{\ell_z} N_i \, \mathrm{d}\Omega \; ;
\tag{12}
$$

$$
\hat{m}_{pj} = \int_{\Omega_p} \frac{N_p}{S_p} \ell_z \left( u_x \frac{\partial N_j}{\partial x} + u_y \frac{\partial N_j}{\partial y} \right) \mathrm{d}\Omega \; ;
\tag{13}
$$

$$
\tilde{m}_{aj} = -\int_{\Omega_a} \sigma \left( u_x \frac{\partial N_j}{\partial x} + u_y \frac{\partial N_j}{\partial y} \right) \mathrm{d}\Omega \; ;
\tag{14}
$$

$$
\hat{l}_{pj} = \int_{\Omega_p} \mathrm{j}\omega\ell_z \frac{N_p}{S_p} N_j \, \mathrm{d}\Omega \; ;
\tag{15}
$$

$$\tilde{l}_{aj} \quad = \quad - \int_{\Omega_a} \mathrm{j}\omega\sigma N_j \, \mathrm{d}\Omega \ . \tag{16}$$

$\ell_z$ is the model length. $\Omega_p$ and $\Omega_a$ are the parts of $\Omega$ corresponding to the stranded conductor $p$ and the solid conductor $a$ respectively. $N_q$ and $S_q$ are the number of turns and the cross-section of the stranded conductor $q$. $r_{pq}$ is the resistance matrix associated with the stranded conductors and the circuit components put in series to them. $g_{ab}$ is the admittance matrix associated with the solid conductors and the circuit components put in parallel to them. $\underline{v}_p$ are the voltages of the sources exciting the stranded conductors. $\underline{i}_q$ is the current through stranded conductor $q$. $\underline{u}_b$ is the voltage drop along solid conductor $b$. A more general treatment embedding the solid and stranded conductors in an arbitrary circuit is presented in [10].

## 5   Non-linear loop with underrelaxation

Ferromagnetic materials offer high permeabilities and are therefore commonly applied in technical devices. Ferromagnetic saturation has a large influence on the device behaviour and hence, has to be faced in the simulation. At elevated speeds, large magnetic flux densities occur at the downwind boundaries which gives rise to substantial saturation and additional leakage flux. For time-harmonic simulation, an effective saturation characteristic is used [11]. The non-linear material characteristic can be introduce in the simulation by the Newton-Raphson technique [12] and the successive approximation method. Here, the second approach is chosen. The reluctivity $\nu$ in (5) is adjusted between successive solutions of linearised systems as in (10). A superscript $(m)$ indicates the non-linear iteration step. The local occurrence of highly saturated material causes a poor convergence of the non-linear loop. An underrelaxation factor $\alpha^{(m)} < 1$ is applied to the successive solutions:

$$\underline{A}_{z,j}^{(m+1)} = \alpha^{(m)} \underline{\tilde{A}}_{z,j}^{(m)} + \left( 1 - \alpha^{(m)} \right) \underline{A}_{z,j}^{(m)} \tag{17}$$

with

$$\begin{bmatrix} \underline{\tilde{A}}_{z,j}^{(m)} \\ \underline{\tilde{i}}_q^{(m)} \\ \underline{\tilde{v}}_b^{(m)} \end{bmatrix} \tag{18}$$

the solution of (10) with the reluctivities $\nu^{(m)}$. $\alpha^{(m)}$ is adaptively chosen out of the set $\{1/2^n \, ; n = 0, \dots, 4\}$ by minimising the non-linear residual

$$\left\| \left( k_{ij}^{(m+1)} + m_{ij} + l_{ij} \right) \underline{A}_{z,j}^{(m+1)} + \hat{f}_{iq}\underline{\tilde{i}}_q^{(m)} + \tilde{f}_{ib}\underline{\tilde{v}}_b^{(m)} \right\|_2 \ . \tag{19}$$

where $k_{ij}^{(m+1)}$ is built by substituting the reluctivities $\nu^{(m+1)}$ in (5).

## 6   Rotational magnetic brake

A rotational magnetic brake consists of a stator yoke with four poles and a solid iron rotor (Fig. 2a). The stator windings excite a four-pole DC air gap magnetic field. The
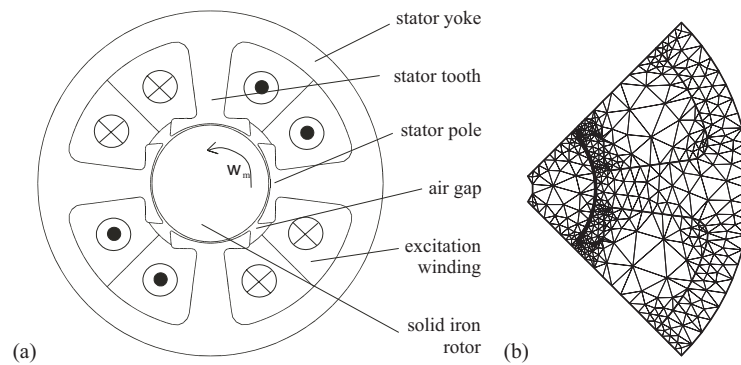
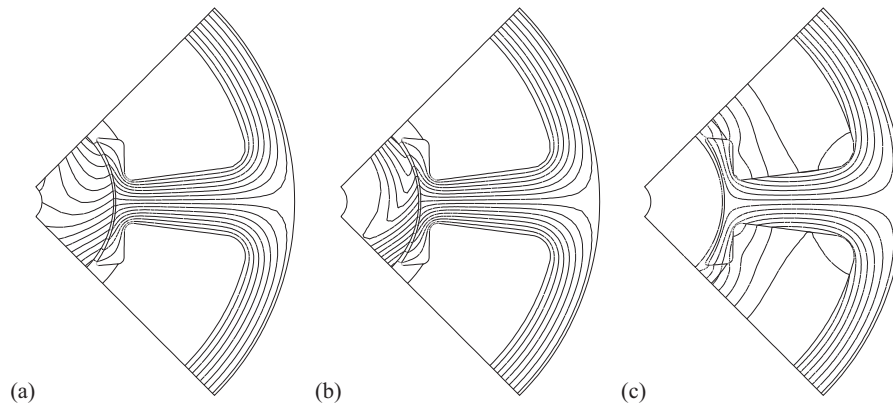Figure 2: (a) Cross-section of a rotational magnetic brake and (b) initial finite element mesh.



Figure 3: Rotational magnetic brake: computed magnetic flux lines for the magnetic brake with the rotor rotating at (a) 1 rad/s, (b) 10 rad/s and (c) 100 rad/s.

rotor is a conductive solid iron cylinder. The magnetic properties of the iron are highly non-linear. The pole shoes are designed to spread the magnetic flux over a large area on the surface of the conductive, soft iron cylinder. The symmetry of the geometry and the excitation enables the application of a reduced 2D model considering one pole pitch with periodic boundary conditions (Fig. 2b).

For large excitation currents, the saturation of the rotor iron causes some leakage flux between the stator poles. As the speed increases (from left to right in Fig. 3), the magnetic flux lines are pushed towards the surface of the solid iron rotor. Because of ferromagnetic saturation, it is not possible to build up a dense flux pattern. As a consequence, the flux in a ferromagnetic brake is more distributed towards the rotor inside and the air gap than for the case of a similar, but non-ferromagnetic brake.

The torque generated by the brake depends on the rate of flux coupled between the stator and the rotor. The torque is computed by an improved Maxwell stress tensor
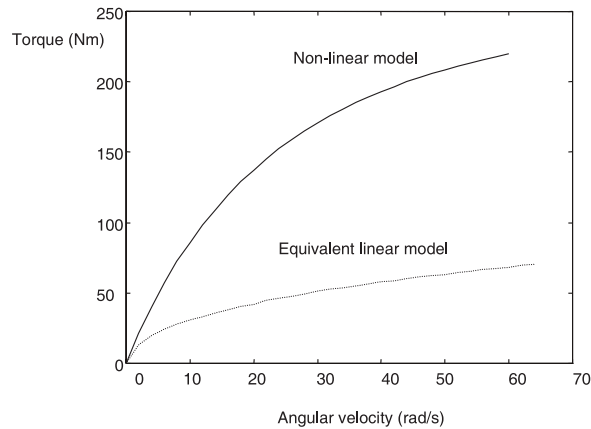
6

Figure 4: Speed-torque characteristic of the rotational magnetic brake.

method [13]. The torque is substantially influenced by the saturation. The ferromagnetic saturation is responsable for a larger torque compared to a brake with an equivalent, but linear magnetisation characteristic (Fig. 4). This technical example shows the importance of non-linear simulation and sufficiently small meshes at the skin layer of moving bodies.

# 7  Solid-rotor single-phase induction machine

The second example is the solid-rotor single-phase induction machine proposed as the Testing Electromagnetic Analysis Methods (TEAM) Workshop problem #30 [14][15]. The solid rotor consists of an iron core covered by an aluminum layer (Fig. 5a). The stator contains a single-phase winding and an iron yoke. The winding is not embedded in slots to enable a comparison with the analytical solution derived in [15]. In this example, all material characteristics are linear. Because of the uniformity of the rotor, transient simulation can be avoided by applying the formulation proposed in this paper. The alternating field excited by the single-phase winding is extreme at a certain time instant $t_0$ (Fig. 5b). At $t_1$, a quarter of a period later, the observed flux is the reaction field of the aluminum rotor part (Fig. 5c). The latter is, however, considerably smaller than the former. The motional formulation is applied for different velocities to compute the speed-torque characteristic of the device (Fig. 6). The results match the analytically determined values.

# 8  Conclusions

For devices featuring uniformly moving bodies, the steady-state simulation of motional eddy currents is based on a motional, time-harmonic formulation. Adaptive mesh refinement combined with an upwinding technique overcomes the numerical problems
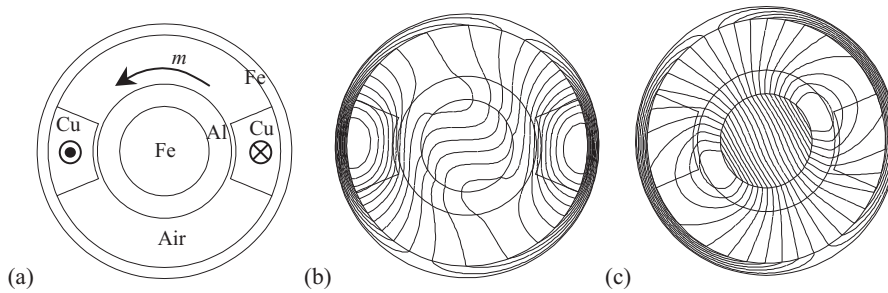
Figure 5: Solid-rotor single-phase induction machine: (a) geometry, (b) magnetic flux lines at $t_0$ and (c) magnetic flux lines at $t_1$.
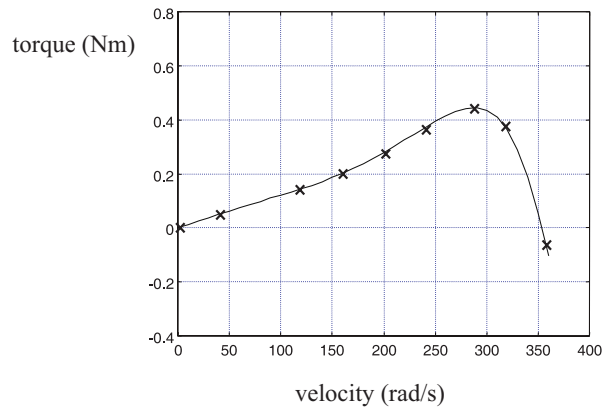


Figure 6: Speed-torque characteristic of the solid-rotor induction machine (the crosses indicate the analytical solution of [15]).

typical for motional partial differential equations. An external electric circuit coupling and a non-linear iteration loop join the formulation and enable its application to technical devices. The method is successfully applied to a magnetic brake with a ferromagnetic rotor and a solid-rotor single-phase induction machine.

# Acknowledgment

# References

[1] A. Sommerfeld. *Electrodynamics*. Academic Press New York, New York, 1952.

[2] T.W. Nehl, B. Lequesne, V. Gangla, S.A. Gutkowski, M.J. Robinson, and T. Sebastian. Nonlinear two-dimensional finite element modeling of permanent magnet eddy current coupling and brakes. *IEEE Transactions on Magnetics*, 30(5):3000–3003, September 1994.

[3] Y.K. Shin and W. Lord. Numerical modeling of moving probe effects for electromagnetic nondestructive evaluation. *IEEE Transactions on Magnetics*, 29(2):1865–1868, March 1993.

[4] H. De Gersem, R. Mertens, and K. Hameyer. Comparison of time-harmonic and transient finite element models for asynchronous machines. In *Proceedings of the International Conference on Electrical Machines (ICEM00)*, volume 1, pages 66–70, Helsinki, Finland, 2000.

[5] D. Rodger, P.J. Leonard, and J.F. Eastham. Modelling electromagnetic rail launchers at speed using 3D finite elements. *IEEE Transactions on Magnetics*, 27(1):314–317, January 1991.

[6] E.R. Laithwaite. *Induction Machines for Special Purposes*. Newnes, London, 1966.

[7] Y. Saad. *Iterative Methods for Sparse Linear Systems*. PWS Publishing Company, Boston, 1996.

[8] K.W. Morton. *Numerical Solution of Convection-Diffusion Problems*. Chapman and Hall, London, 1996.

[9] H. Vande Sande, H. De Gersem, and K. Hameyer. Finite element stabilization techniques for convection-diffusion problems. *7th International Journal of Theoretical Electrotechnics*, pages 56–59, March 1999.

[10] H. De Gersem, R. Mertens, U. Pahner, R. Belmans, and K. Hameyer. A topological method used for field-circuit coupling. *IEEE Transactions on Magnetics*, 34(5):3190–3193, September 1998.

[11] D. Lederer and A. Kost. Modelling of nonlinear magnetic material using a complex effective reluctivity. *IEEE Transactions on Magnetics*, 34(5):3060–3063, September 1998.

[12] D. Lederer, H. Igarashi, and A. Kost. The Newton-Raphson method for complex equation systems. In *Proceedings of the 7th international IGTE symposium on numerical field calculation in electrical engineering (IGTE98)*, pages 391–394, Graz, Austria, September 1996.

9

[13] K. Hameyer, R. Mertens, U. Pahner, and R. Belmans. New technique to enhance the accuracy of 2-d/3-d field quantities and forces obtained by standard finite-element solutions. *IEE Proceedings Science, Measurement and Technology*, 145(2):67–75, March 1998.

[14] Testing electromagnetic analysis methods (TEAM). http://www.lmn.pub.ro/networks/team/.

[15] K. Davey. Analytic analysis of single- and three-phase induction motors. *IEEE Transactions on Magnetics*, 34(5):3721–3727, September 1998.